

Semi-Annual Report Submitted to the
National Aeronautics and Space Administration

For July - December, 1998

Contract Number: NAS5-31370
Land Surface Temperature Measurements
from EOS MODIS Data

MODIS Team Member
PRINCIPAL INVESTIGATOR

ZHENGMING WAN

P.I.'s Address:

Institute for Computational Earth System Science
University of California
Santa Barbara, CA 93106-3060

phone : (805) 893-4541
Fax no: (805) 893-2578
Internet: wan@icess.ucsb.edu

Land Surface Temperature Measurements from EOS MODIS Data

Semi-Annual Report for July - December, 1998

Zhengming Wan

Abstract

We present a strategy of vicarious calibration for the thermal infrared channels of airborne and satellite sensors and its requirements for in-situ measurements of the atmospheric and surface parameters. This strategy has been applied to the MAS data acquired in the field campaign conducted in Mono Lake, California on March 10, 1998, because of the calm clear-sky and dry atmospheric conditions. The MAS data quality was evaluated over four test areas: a portion of Grant Lake covered by thin ice with melting edges, a portion of Grant Lake covered by snow, a portion of Mono Lake, and a snow field between these two lakes. Field measurements were made over the snow-cover site for land-surface temperature with TIR spectrometer and radiometers, for atmospheric temperature and water vapor profiles with radiosonde. The estimated MAS noise-equivalent temperature difference is 0.6-1.2°C for bands 30-32 in the 3.5-4.2 μ m region, 0.1-0.5°C for bands 42, 45, 46, and 48 in the 8-13.5 μ m region. Atmospheric radiative transfer simulations indicate that the effects of uncertainties in measured atmospheric water vapor and temperature profiles on the brightness temperature in these seven MAS bands are small or moderate under the dry atmospheric condition and that these effects would be even smaller if the surface elevation is over 4km above the sea level. We used the spectral emissivity value of the Krylon ultraflat black paint measured in laboratory to recalibrate the MAS 1B data. This recalibration changed the brightness temperatures in the seven bands by an amount ranging from -0.42 to 0.33°C over the ice-covered Grant Lake. We analyzed the effects of uncertainties in surface temperature and emissivity on the results of the vicarious calibration. This study indicates that the MAS calibration accuracy for the split-window channels (at 11 and 12 μ m) has been significantly improved (to better than 0.3°C) in the past three years while the calibration accuracy in other TIR channels needs further improvement. We also present a plan of vicarious calibration activities for MAS and MODIS TIR channels by the use of homogeneous targets at high elevations in the coming years.

Recent Paper Published

W. Snyder, Z. Wan, Y. Zhang and Y.-Z. Feng, "Classification-based emissivity for the EOS/MODIS land surface temperature algorithm", *Int. J. Remote Sensing*, Vol. 19, No. 14, pp. 2753-2774, 1998.

1. INTRODUCTION

The Moderate Resolution Imaging Spectroradiometer (MODIS) has been developed as the keystone instrument (Salomonson et al, 1989; Barnes et al, 1998) on the EOS (Earth Observing System) AM-1 platform (King et al, 1995) for global studies of atmosphere, land, and ocean processes (King et al, 1992; Justice et al, 1998; Esaias et al, 1998). In order to support the validation of MODIS algorithms and data products, the MODIS Airborne Simulator (MAS) has been developed for the NASA's high-altitude ER-2 research aircraft as an outgrowth of the development of the Wildfire infrared imaging spectrometer which was originally designed for investigations of high-temperature terrestrial targets such as forest fires. King et al (1996) described its technical details, calibration method, and performance evaluation of the MAS instrument.

Beginning in January 1995, a 50-channel, 16-bit digitizer was used, which greatly enhanced the capability of MAS to simulate MODIS data over a wide range of environmental conditions. The dynamic range of the TIR channels is wide enough to encompass cold cloud targets as well as warm terrestrial surface targets. MAS has a spatial resolution of 50m (pixel size) at the sea level when on the ER-2 research aircraft flying at altitude of 20km. Radiometric calibration of the shortwave MAS channels is obtained by observing laboratory standard integrating sphere sources on the ground before and after flight missions, while calibration of the infrared channels is performed in flight by viewing two onboard blackbody sources once every scan. The new calibration method (King et al, 1996) takes into account the effect of blackbody emissivity. In the preliminary MAS 1B processing, the calibration of MAS thermal infrared data was based on the effective blackbody emissivity values determined by regression analysis of the laboratory observations of a thermally controlled external source in a stable ambient environment (Moeller et al, 1996).

MAS in its March 1998 configuration has 50 narrowband channels shown in Table I in the spectral range between $0.47\ \mu\text{m}$ and $14.5\ \mu\text{m}$, 10 of the shortwave channels ($< 2.5\ \mu\text{m}$) similar to the MODIS reflective channels, and 12 of the emissive channels similar to the MODIS thermal infrared (TIR) bands at approximately same wavelength locations including the seven MODIS TIR bands (bands 20, 22, 23, 29, and 31-33) used in the MODIS land-surface temperature (LST) algorithms (Wan and Dozier, 1996; Wan and Li, 1997).

In this paper, we present the strategy of vicarious calibration for the seven MAS bands used in LST remote sensing and its requirements for in-situ measurements of the atmospheric and surface parameters in section 2. We describe the MAS flights and field measurements in the March 1998 field campaign conducted in Mono Lake, California in section 3, and present the vicarious calibration results in section 4. Conclusion and the MODIS LST plan for calibration/validation activities are given in section 5.

2. STRATEGY OF VICARIOUS CALIBRATION FOR TIR CHANNELS

In the past several years, we made great efforts into the development of a calibration/validation strategy plan and TIR instrumentation for the validation of the MODIS LST algorithm and products. Vicarious calibration (i.e., validation of the TIR calibration through in-situ measurements) of MAS and MODIS TIR channels is a critical part of this strategy plan because the quality of the MODIS LST products depends not only on the quality of the LST algorithm but also on the calibration accuracy of the TIR channels used in the MODIS LST algorithm.

The validation is a comparison between temperatures retrieved from in-situ measurements and those retrieved from airborne and satellite thermal infrared data. Large homogeneous test sites such as silt playas and inland lakes have been chosen because their in-situ surface temperatures can be measured more accurately. These test sites validate primarily the atmospheric correction and emissivity-extraction portions of the MODIS LST algorithms. Validation requires in-situ measurements of surface temperature at accuracy better than 1 °K (with a goal of 0.6 °K), the specified accuracy for MODIS LST products. Vicarious calibration of TIR channels has higher accuracy requirements for ground-based measurements of surface-leaving radiance (or surface temperature and emissivity), and for the measurements of atmospheric temperature and water vapor profiles. The overall error associated with uncertainties in ground-based surface parameters and atmospheric profiles, and in the atmospheric radiative transfer simulation based on measured atmospheric and surface conditions should be smaller than 0.5% in order to be able to validate the calibration accuracy (0.5 to 1.0%) of the MODIS TIR channels (Butler and Barnes, 1998). In section 4, we will show that vicarious calibration needs to use high-elevation test sites under dry atmospheric conditions

The in-situ measurements have spectral, spatial, temporal, and angular requirements. For the spectral requirements, spectral emissivities of surface cover types need to be measured in order to validate the recovered band-averaged surface emissivities. For spatial requirements, product validation needs to be carried out for different land cover types and different latitudes. This sampling should include a range of surface temperatures and atmospheric conditions. The land cover types will include prototypes of the main groups such as desert, bare soil, crop-land, grassland, forests, water, snow and ice. For unstructured surfaces, the in-situ measurements can be made with transects large enough to represent the aerial pixel average. For structured surfaces, tower or aerial measurements will be required. Ideal test sites are flat areas with size larger than 3km by 3km with uniform or uniformly mixed surfaces so that the uncertainty in spatial sampling is significantly reduced. For in-situ measurements, the short-term changes in temperature are difficult to quantify, so weather conditions for such measurements must be stable (constant wind speed). We have analyzed validation requirements versus spatial and temporal variations of surface temperature for a silt playa (Snyder, et al., 1997a). The requirements for long-term temporal sampling depend on latitude, and can be combined with the requirements for spatial sampling. In other words, we

need a seasonal and global range of surface temperatures and atmospheric conditions. Finally, the surface measurements should be made at the MODIS/MAS look angle. Therefore, in-situ measurements should be made at multiple viewing angles in order to ensure the radiance or temperature at the MODIS/MAS viewing angle can be interpolated accurately. For daytime measurements, a range of sun angles also must be incorporated for validation of the mid-infrared band processing and for validation of the mixed-temperature model with structured surfaces.

The metric for measures of success for validation will be the difference between the surface temperature estimated from in-situ measurement data and that retrieved from airborne or satellite data. Because there are errors in both the ground measurements and the satellite measurements, the success criterion will depend on the ground measurement accuracy as well as the accuracy of airborne and satellite data. The success criterion will also depend on atmospheric and surface conditions. It is critical to have high quality ground measurements with small temporal and spatial variations in order to reduce the uncertainties in temporal interpolation, spatial sampling, and geometric co-registration. In-situ measurements should include records of the atmospheric and surface weather conditions. After collection, an error analysis of in-situ measurements and the aerial and satellite measurements is required to determine the potential validation accuracy. The LST product will be considered valid when the measurements and error analysis indicate an absolute accuracy of the aerial or satellite measurements of better than 1 °K standard deviation.

Surface temperature measurements can be made with contact sensors, portable infrared thermometers as wideband radiometers, and infrared spectrometers. Transects will be made with infrared thermometers. The contact sensors are thermistors with dataloggers for surface temperature measurements of water body and flat land surfaces such as the silt playa 1-2mm beneath the surface. Temperature is recovered directly from the contact sensors. We use the TIR thermometer manufactured by Heimann as the broadband radiometer. The spectrometers do not translate easily, but they can scan a range of angles to provide temporal and angular spectral surface radiance and atmospheric downwelling radiance (from a diffuse reflector). The TIR spectrometer (from MIDAC Corp.) equipped with InSb/MCT sandwich detector can provide radiance data at a selectable spectral resolution of 1 to 32 wavenumbers in the spectral range 3.5-14.5 μ m. Normally we select the 4 wavenumber resolution in our field measurements. At this spectral resolution, the speed of the spectrometer is 8 spectra per second. We made a series of custom improvements to this TIR spectrometer, including installation of a beam expander, a scanning mirror and three blackbody boxes in the front of the spectrometer. The field-of-view (FOV) of this improved TIR spectrometer is approximately 25cm when it is placed at a platform 3m above the ground. This TIR spectrometer with the scanning mirror can scan a range of angles to provide temporal and angular spectral surface radiance and atmospheric downwelling irradiance (with a diffuse reflector). The measured downwelling irradiance has been used in the atmospheric correction of the ground-based measurement data. These TIR instruments are calibrated with a full aperture blackbody in a range of temperature wide enough to cover the surface temperature conditions in the field. An aluminum-foil cone is placed in front

of the blackbody aperture in order to isolate the blackbody from the environmental radiation and TIR instruments view the blackbody surface through the aluminum-foil cone. We also use water bathed cone blackbody to check the accuracies of our TIR instruments (including the full aperture blackbody) routinely. High precision thermistors (with accuracy better than 0.1 °C) used in blackbodies provide the traceability to the NIST standard. The accuracies of thermistors and TIR radiometers are ± 0.2 °C. Multiple sets are used in order to obtain a better accuracy. The accuracy of the TIR spectrometer is better than 0.15 °C in the 8-14 μm range. In this spectral range the signal-to-noise ratio (SNR) of a single spectrum of the TIR spectrometer is larger than 1000. At least 256 sets of spectra are averaged in order to obtain high SNR in the medium wavelength range down to 3.5 μm .

Spectral directional-hemispherical emissivity can be measured with an integrating sphere facility which includes a Fourier transform infrared (FTIR) spectrometer and a 5-inch infragold integrating sphere. The spectrometer has sensitivity both in the mid and thermal infrared, covering all MODIS bands of interest for LST. This instrument is primarily used for emissivity measurements of samples such as ice, water, silt, sand, soil, leaf surface, and etc. Laboratory and field measurements of the infrared BRDF (bidirectional reflectance distribution function) and emissivity can also be made with the UCSB SIBRE (Spectral Infrared Bidirectional Reflectance and Emissivity) instrument, which includes a hemispherical pointing system, a FTIR spectrometer, a TIR source, and reference plates (Snyder et al, 1997b). The effect of surface temperature change due to the thermal source heating is carefully corrected (Snyder and Wan, 1996). The spot size viewed by the SIBRE instrument is approximately 3cm in diameter so materials with some small-scale surface structure can be examined. We also have a beam expander that gives a 12cm spot for more structured surfaces. We can recover angular spectral emissivity from absolute radiance measurements using a sun-shadow technique which is similar to the day/night method.

Vicarious calibration of MAS TIR channels is important for the following reasons: 1) It is relatively easier to make in-situ measurements at the MAS pixel scale than the MODIS pixel (1km) scale. 2) Once MAS calibration is validated, it can be used to validate the calibration accuracy of MODIS TIR channels. 3) MAS data will be used to validate MODIS LST products in areas with heterogeneous land-cover types in complicated terrains where it is almost impossible to obtain accurate ground-based measurement data at the MODIS pixel scale.

3. THE MARCH 1998 FIELD CAMPAIGN WITH MAS FLIGHTS

We have conducted six field campaigns with MAS flights for the validation of MODIS LST algorithms in Railroad Valley, Nevada and in the area of Mono Lake and Mammoth Lake, California during 1995-1998. Although these field campaigns provided useful data for the LST validation purpose (to validate LST algorithm at the 1 °K accuracy), we found that only the data collected in the last field campaign conducted in Mono Lake in March 1998 can be used for vicarious calibration of the MAS thermal channels.

We requested two weeks of MAS flight opportunity for the March 1998 field campaign. The MAS flight lines were selected in the north-south direction, covering Mono Lake, snow in mountains and valleys, and forest areas. Details of the MAS flight lines can be found in flight numbers 98-032 and 98-033 on the web page of the NASA Ames Research Center (http://asapdata.arc.nasa.gov/ames_index.html). Five groups were interested in this field campaign, two from the MODIS Team, one from the AirMISR team, and two groups of validation scientists. Unfortunately, two groups could not participate because we got the announcement of the confirmed flight schedule only ten days before the first possible flight on March 9, 1998.

On March 9, 1998, the ER-2 Operation Office at NASA Dryden Flight Research Center and the Earth Science Division at NASA Ames conducted a test flight for the MAS instrument after its maintenance service. March 10, 1998 was a very nice day with clear-skies. The measured wind speed was less than a half meter per second. The daytime MAS flight passed the Mono Lake area around 11:30 PST. Since the sky remained clear until early evening, we decided to conduct the night MAS flight mission on the same day. The night MAS flight passed the same area at around 10pm PST. We observed some light haze moving slowly in the sky, which was more obvious in the far distant mountains. Two radiosonde balloons were launched, one for the daytime MAS flight, and another for the night MAS flight. The measured atmospheric temperature and water vapor profiles are given in Fig. 1. The column water vapor calculated from the profile is 0.32cm for the daytime flight and 0.38cm for the nighttime flight.

We performed ground measurements at a site in the snow field approximately 1 km from the crossing of Highways 395 and 120 in the east, and 70 m from Highway 120 in the north side. This snow site and other interesting sites are shown in Fig. 2 of the MAS image which we will discuss in more detail in a later section. We used one MIDAC TIR spectrometer to measure temporal TIR radiance from the snow surface. The spectrometer scanned from east to west at viewing angles 30 to -30 degree in steps of 15 degree. Six broadband radiometers (in wavelength range 10-13 μm) were placed 2 m above the surface to measure the snow surface temperature. Six thermistors were placed a few mm beneath the snow surface to make the contact measurement of the near-surface snow temperature. The distance between individual radiometers and thermistors was approximately 50 m. We recorded measurement data from these field instruments throughout the day and night on portable computers and data loggers. The analysis and comparison of the measurement data from MAS and field instruments can be found in the following sections.

In this study, we used only the daytime MAS data to avoid the uncertainty caused by the night haze and thin cirrus clouds. We enhanced the daytime MAS images in bands 30, 42 and 45 with the histogram equalization method, and then made a color composite image with bands 45, 42 and 30 as red, green and blue components. Fig. 2 is the black-white copy of the color composite. The left image (a), composed of 1000 lines with each line containing 716 pixels, covers an area of approximately 45km in N-S direction and 32km in the E-W direction. Each pixel represents a spot of approximately 45 m by 45 m (due to the

surface elevation being approximately 2 km in the region) on the ground. The band brightness temperature given in these TIR band images is calculated from the pixel radiance value calibrated by the new method (King et al., 1996), which uses the MAS relative spectral response functions and corrects the effect of the non-unit blackbody emissivity. The radiance to temperature conversion is given by the adjusted Planck function

$$I_b = B(\lambda_b, \alpha_1 T_b + \alpha_0). \quad (1)$$

where I_b is the band radiance, T_b is the band brightness temperature. The values of the central wavelength λ_b , coefficients α_1 and α_0 for band b are all given in the MAS 1B data file.

Mono Lake, Highways 395 and 120, Mono Craters, and the forest areas are shown clearly in the image. Mono Lake is on the top. Highway 395 is the white line crossing the image from upper left corner to the lower right corner. The white line crossing Highway 395 in the north-west direction is Highway 120. The white areas with dark points inside located in the middle portion of the image are the Mono Craters. The grey areas with non-uniform grey levels in the lower right portion are the forest areas. Mono Lake and forest areas are in light yellow in the color composite image. Fig. 2(b), the right image, is the enlarged sub-area for showing four test areas used in this study. Grant Lake is in the lower left corner. The upper part in light dark grey is the part covered with snow, and the lower part in dark grey is the part covered by thin ice on 10 March 1998. The near infrared color film taken with 6" RC-10 (CIR) camera on the same ER-2 aircraft carrying the MAS instrument indicates that the thin ice cover on Grant Lake was in the state of melting because we can see some strips in the ice area and some small blocks of water surface in black by the edge. The dark grey area between Highways 396 and 120, in the middle of this image, is the snow field site where we made field measurements. A portion of Mono Lake (80 by 80 pixels) in the upper right corner is another study area.

4. RESULTS

4.1. Noise Equivalent Differential Temperature ($NE\Delta T$) of MAS TIR Channels

The focus of this study is on the seven MAS TIR bands (bands 30-32, 42, 45, 46, and 48) that are used in the MODIS LST algorithm. Investigation of other TIR bands needs measurement data for the atmospheric temperature and water vapor profiles above elevation 9km above the sea level and for other atmospheric parameters including ozone profile, which were not available from this field campaign. In order to check the radiometric accuracy of the MAS TIR data in these seven bands, we calculated the average band brightness temperatures and standard deviations of the day MAS data over four flat homogeneous study areas: two on Grant Lake (one covered with ice and the other with snow), one on Mono Lake, and another on the snow field site, as shown in Table II. The sizes of the study areas are 80 by 80 pixels for the one on Mono Lake, and 16 by 16 pixels for others. The first and second columns of Table II contain the band number and band centers λ_b respectively, while columns 3-6 are the mean and standard deviation (in the

parentheses) of band brightness temperature T_b . The estimated minimum and maximum $NE\Delta T$ values are shown in the last two columns. The spatial variations of T_b in each of the study areas may have been affected by the variations in surface temperature, surface reflectivity and emissivity, and in atmospheric temperature and water vapor profiles. The variations caused by the surface were minimized by the flatness and homogeneity of the selected study areas. Correlation analysis for the study areas rejected the assumption that the variations in T_b were caused by the variations in surface temperature and emissivity. We used the T_b values of each pixel in bands 42 and 30 as independent variables and used the T_b values in other bands as dependent variables. The atmosphere is assumed to be uniform over the study area in this analysis. With T_b of band 42 representing the spatial variation in surface temperature and the T_b of band 30 representing the spatial variation in surface reflectivity and emissivity, we would have found nearly perfect correlation of the dependent variable with the independent variables, i.e., the residual difference between the measured T_b value and the value calculated from the correlation would be very small. However, our analysis indicates that it is not true for the T_b data sets of these study areas. Therefore, the major component in δT_b values in Table II is due to the noise of the MAS instrument. It appears that real surface temperature varies by 0.1-0.2°C in these flat homogeneous study areas and that the remaining common part is $NE\Delta T$ as shown in Table II.

4.2. Effects of the Uncertainties in Measured Atmospheric Profiles

We made atmospheric radiative transfer simulations with the version 3.5 of the MODTRAN code (Berk et al., 1987) for the ice-covered Grant Lake surface (at elevation 2 km) based on the atmospheric temperature and water vapor profiles measured during the day flight. Above the altitude (8-9km) where our radiosonde stopped to provide profile data, we used the standard winter mid-latitude atmospheric profiles in the MODTRAN code. Radiative transfer simulations showed that the effect of changes in the temperature and water vapor profiles above 9km is negligible for the seven MAS TIR bands of our interest. We assumed that the thin-ice surface temperature was -0.5°C and that it reflected solar radiation and downward atmospheric thermal radiative flux as a specular surface. The reflectivity of a smooth ice surface could be calculated from the complex index of refraction for ice (Warren, 1984). The standard rural aerosol profile in the high visibility condition was used in our simulations. The effect of change in aerosol density in this high elevation case should be negligible because the atmosphere was so dry and the visibility was extremely high. The band brightness temperatures (T_b) given by the atmospheric radiative transfer simulations in the seven MAS TIR bands are given in Table III. The simulated T_b values based on the measured atmospheric profile are given in the third column. The simulated T_b values based on adjusted profiles (one for doubling the water vapor, another for shifting the temperature profile by 2°C) are given in the next two columns. Because we started the first radiosonde measurement at 10:58 PST and the MAS flight passed the Grant Lake at 11:30 PST, the increase of the atmospheric temperature by 2°C in the lower portion of the temperature profile can be justified. The changes due to the adjustments on column water vapor and temperature profile are shown in parentheses. Due to the dry atmospheric condition, the effect

of doubling the column water vapor on the band radiance at the top of the atmosphere seems to be very small in all seven bands. This effect is evident in the maximum value of -0.13°C , in band 42, the same level of $NE\Delta T$ in this band. Because of the dry atmosphere and the relative high surface elevation, the effect of changes in atmospheric temperature profile on T_b appears to be moderate, less than 0.6°C in band 48 at the worst. If we were to lift the measured atmospheric temperature and water vapor profiles by 2km so that the surface elevation becomes 4km above the sea level, the effect of changes in atmospheric temperature profile on T_b would be reduced by more than 20% in bands 30-32, 42 and 48.

4.3. Recalibration with Measured Blackbody Emissivity

As described by Eq. (3) in the paper of Moeller et al (1996), the equation for non-unit emissivity calibration of MAS thermal infrared data in the preliminary MAS 1B processing is

$$R_o = \varepsilon_b [(C_o - C_a) \frac{(R_w - R_a)}{(C_w - C_a)} + (R_a - R_r)] + R_r \quad (2)$$

where R_o and C_o refer to observed scene radiance and digital count, R_w and R_a refer to warm and ambient blackbody radiances, C_w and C_a refer to warm and ambient blackbody counts, ε_b representing the effective blackbody emissivity for channel b, and R_r representing the background radiance reflected by the blackbody. The reflected R_r is dominated by radiance from the MAS instrument hardware. In the above equation, we omitted the explicit unknown error terms. The value of ε_b (0.98 for SWIR channels and 0.94 for LWIR channels) was determined by regression analysis of the laboratory observations of a thermally controlled external source in a stable ambient environment.

We measured the spectral emissivity of the Krylon ultraflat black paint that was used to paint the MAS blackbodies and found that the measured emissivity values were different from these effective blackbody emissivity values. From Eq. (2), the effect of emissivity change on scene radiance is

$$\delta R_o = \frac{\delta \varepsilon_b}{\varepsilon_b} (R_o - R_r) . \quad (3)$$

We can calculate R_r from the measured instrument background temperatures given in the 1B data file. Letting $\delta \varepsilon_b$ be the difference between the measured ε_b and the effective emissivity value, we get the recalibrated scene radiance as

$$R_o' = R_o + \frac{\delta \varepsilon_b}{\varepsilon_b} (R_o - R_r) . \quad (4)$$

This allows us to calculate the recalibrated brightness temperature T_b from R_o' . As shown in Table IV, this recalibration changed the brightness temperatures in the seven bands by an amount ranging from -0.42 to 0.33°C over the ice-covered Grant Lake. Similarly, this recalibration is also made for other study areas. The results are shown in Table V. The recalibration reduced the mean, maximum, and rms calibration

errors in the seven bands by more than 10% in case of the Mono Lake study area.

4.4. Comparison with Ground-based Measurements over a Snow Field

Six thermistor-dataloggers, six TIR thermometers, and one TIR spectrometer were used to measure the snow surface temperature over the snow field between Mono Lake and Grant Lake. With the sunshine causing the snow to melt, the thermistors lost contact with snow particles. As a result, the thermistors gave the air temperature rather than the snow surface temperature. According to specifications, the Heimann thermometers should work when the ambient temperature is above 0 °C and would not work below 0 °C without heating. Around the MAS overpass time (11:29am PST), the surface air temperature was 3 °C. Only three Heimann thermometers worked appropriately, giving average temperature to be -1.92 °C when emissivity was set to 1.0 for the thermometers. This brightness temperature could be converted into surface radiometric temperature by correcting the effects of surface emissivity and the downward atmospheric radiation. The effect of reflected downward atmospheric radiation is negligible in this case of very dry atmospheric condition above surface elevation 2km.

The spectral emissivities of water, snow, and ice are shown in Fig. 3. The water emissivity (solid line), and ice emissivity (dots) are calculated from the complex index of refraction (Hale and Querry, 1973; Warren, 1984) at MAS viewing angle 1.4° for the Mono Lake study area and 23.2° for ice-covered Grant Lake, respectively. The spectral emissivity of snow was obtained by measuring snow samples with our spectrometer-integrating-sphere facility in the cold laboratory at Sierra Nevada Aquatic Research Laboratory in 1995. The measured water emissivity is also included to show the quality of our emissivity measurements (maximum error smaller than 0.002).

The averaged snow emissivity in the spectral window of Heimann thermometers (10-13 μm) is 0.982, corresponding to a temperature correction of 1.0 °C. After the emissivity correction, Heimann thermometers gave a snow surface temperature at -0.92 °C. The TIR spectrometer gave a snow surface temperature at -0.77 °C at viewing angle 15° in the spectral range of MAS band 42 (around 8.5 μm) where snow emissivity has the maximum value to minimize the effect of the uncertainty in snow emissivity. If we average the surface temperature values given by three Heimann thermometers and one TIR spectrometer, the measured snow surface temperature would be -0.84 °C. We realize that four measurements are not enough to perform a full analysis of the spatial variation in snow surface temperature at the 1m scale even though MAS data indicate that surface temperatures over the snow field study area are quite uniform at the 50m scale. The spatial variation in surface temperatures at scale of a few meters will be a major concern to be addressed in future field campaigns.

Atmospheric radiative transfer simulations were made with the measured snow temperature and emissivity, atmospheric temperature and water vapor profiles. The solar zenith angle was 42.3° at the MAS overpass time. The comparison between MAS data and brightness temperatures (T_b) given by radiative transfer

simulation based on measured atmospheric and surface conditions at the MAS viewing angle is shown in the first part in Table V. For MAS bands 30-32, the calculated T_b values were given in ranges based on how snow surface reflects the solar beam. The lower boundary of the T_b range represents the case of a specularly-reflecting snow surface so that there is no contribution from reflected solar beam in the radiance received by the MAS instrument. The upper boundary represents the case where snow surface reflects solar beam, like a Lambertian surface. It is worthy to point out that the MAS T_b value is the average value of 16 by 16 pixels and its precision should be better than 0.1 °C according to the standard deviation values in Table II. The measured snow surface temperature, -0.84 °C is the average surface temperature value of snow at four locations observed by three Heimann thermometers (with FOV 1m) and one TIR spectrometer (with FOV of 25cm). Column 4 in Table V contains the T_b value from original MAS 1B data file. The recalibrated T_b values are given in the last column. The temperature difference (δT_b) between MAS T_b value and the value derived from radiative transfer simulation based on field measurement data is given in parentheses to show the calibration accuracy of MAS TIR channels. As a result, the calibration of MAS channels 45 and 46 is within 0.3 °C before recalibration and 0.1 °C after recalibration. In the following section, we will adjust surface temperature values for other three study areas until δT_b in band 45 smaller than 0.1 °C (because there is no in-situ measurement for their surface temperatures) in order to obtain some statistical characteristics of the MAS calibration in the seven TIR bands.

4.5. Results of Vicarious Calibration in Study Areas Over Grant Lake and Mono Lake

The comparison over the snow-covered Grant Lake is shown in the second part of Table V. We used the same snow surface temperature measured at the snow field site in atmospheric radiative simulations because the difference in T_b values over these two sites is less than 0.05 °C in bands 42 and 45 as shown in Table II, but the viewing angle was set to 23° corresponding to the MAS look angle. We only listed T_b values in bands 30-32 for the case of specular snow surface, i.e., assuming no contribution from the reflected solar beam to the MAS signal.

For the ice-covered Grant Lake site, surface temperature was set to -0.7 °C, and the calculated smooth ice spectral emissivity shown in Fig. 3 was used in the atmospheric radiative transfer simulation under the specular reflection assumption for ice surface. Although the ice surface temperature (-0.7 °C) is slightly above the snow surface temperature (-0.84 °C), the band brightness temperatures in bands 42 and 45 are smaller over the lake ice because the ice emissivity is smaller by approximately 0.01 than snow emissivity in these two bands. There is a question mark after the δT_b value in parentheses for bands 30-32 because the lake ice may not be exactly like a specular reflecting surface for the solar beam due to its unknown surface roughness.

The comparison results over the Mono Lake study area were given in the last part of Table V. As shown in Table II, the Mono Lake study area has the smallest standard deviation values of band brightness temperature (δT_b) in bands 30-32 although δT_b values in bands 42 and 45 are larger than those in other

study areas. This indicates that there were some small spatial variations in the lake surface temperature (about 0.2°C in the area of 4km by 4km) and that the lake surface would be more like a specular reflecting surface because of the extreme low wind speed. For flat water surface, spectral emissivity can be calculated or measured at high accuracies as shown in Fig. 3. The only problem for this field campaign was that we were unable to deploy thermistor-dataloggers at the desirable locations in Mono Lake due to the unavailability of boats at that time. We were only able to deploy two thermistors in the lake surface layer near the lake shore. Because there were much larger spatial variations in water surface temperature by the lake shore, we would not select a study site in the area where thermistors were deployed. After the atmospheric and surface conditions were given by in-situ measurements, the only variable in the inputs to the atmospheric radiative transfer simulations was the water surface temperature. With the excellent agreement between MAS T_b and the derived T_b based on measured atmospheric and surface parameters over the snow field study area in band 45, and the maximum $NE\Delta T$ being only 0.2°C for this band, it is possible to determine the water surface temperature from MAS observation in band 45 through accurate radiative transfer simulations. If we set the water surface temperature at 4.6°C , the derived T_b values would match well with MAS T_b values within 0.1°C for bands 45 and 46.

By comparing the δT_b values in parentheses for the four study areas, they were found within $\pm 0.2^{\circ}\text{C}$ in bands 45 and 46 for all study areas but the ice-covered Grant Lake site. The large δT_b value in band 46 ($\delta T_{b,46} = 0.58^{\circ}\text{C}$) can be explained by the large uncertainty in band emissivity in band 46 (ϵ_{46}) because the calculated spectral emissivity of smooth ice surface reaches its minimal value (0.93) around $12\mu\text{m}$. It is quite reasonable to increase ϵ_{46} by 0.009 since the emissivity should be increased as surface roughness increases in order to match the calculated $T_{b,46}$ with the MAS $T_{b,46}$ value.

4.6. Cross Comparison of the MAS Calibration

Table VI lists the MAS TIR channel calibration errors from this study and two other papers (King et al, 1996; Moeller et al, 1996). Column 3 is for the MAS configuration in March 1998 and the last two columns are for the MAS configuration in 1995. This study shows that the MAS calibration accuracy for the split-window channels (at 11 and $12\mu\text{m}$) has been significantly improved to better than $\pm 0.3^{\circ}\text{K}$ in the past three years while the calibration accuracy in other TIR channels needs further improvement. The values of MAS TIR channel calibration errors in column 3 come from the comparison between the recalibrated MAS T_b value and the derived T_b value based on measured atmospheric profiles for the Mono Lake study area, as shown in Table V, under the assumption that the lake surface temperature can be accurately given by the MAS channel 45 data. This assumption traces to the vicarious calibration based on in-situ measurements over the snow field study area. As indicated in Table III, the effect of uncertainties in measured atmospheric profiles on T_b in channel 45 is smaller than 0.05°C if the accuracy of the measured atmospheric temperature profile at lower levels (from surface up to elevation 9km) is better than 2°C . Therefore, the error in the in-situ measurement of snow surface temperature is the dominant uncertainty

source in the estimation of MAS calibration accuracy.

The error analysis of the snow surface temperatures determined by the MIDAC TIR spectrometer in MAS channels 42 and 45 is shown in Table VII. The calibration accuracy of the spectrometer is better than 0.15 °C. This has been proved by viewing blackbody at different temperatures routinely. The traceability to the NIST standard is provided by the high precision thermistors with accuracy better than 0.1 °C. The effect of uncertainties in measured snow surface emissivity (less than 0.0025) on the surface temperature determination is less than 0.15 °C. The spatial variation in the real snow surface temperature is estimated as 0.2 °C which is referred from MAS data over the snow-field study area as shown in Table II. In this field campaign we do not have strong evidence for this estimation at the scale pertaining to the FOV of the spectrometer. We will use an IR camera continuously to measure the spatial distribution of surface temperature in future field campaigns.

There are two approaches to obtain the band brightness temperature at the top of the atmosphere from in-situ measurements through atmospheric radiative transfer simulations. The band brightness temperature will be used to compare with MAS or MODIS data for the vicarious calibration purpose. The first approach is based on the measured surface emissivity and temperature. The second approach is based on the measured surface-leaving radiance. In the first approach, the uncertainty in measured surface emissivity may be one of the major error sources, depending on the type of land surface. In the second approach, the spectral surface-leaving radiance measured by TIR spectrometers can be directly used as an input to the atmospheric radiative transfer simulations. Currently we take the first approach because we have not found a confident way to separate the measured environmental radiation reflected by the surface into two components, one contributed from the atmospheric radiation, another contributed from the platform which supports the TIR spectrometer. Most recently we have made some structural changes of the platform to reduce its environmental radiation. If we can separate the second component from the total reflected environmental radiation accurately, we will be able to take the radiance-based approach. Then we will be able to achieve the accuracy ± 0.15 °C (shown in parentheses in column 3 of Table VI), the goal of the MAS vicarious calibration in channels 45 and 46 under ideal surface and atmospheric conditions.

5. CONCLUSION

This study shows that the MAS TIR channel calibration can be validated with in-situ measurements at an accuracy better than 0.5% for channels 30-31 and 45-46, and better than 1% for channels 32, 42 and 48 over flat homogeneous test sites under the following conditions: surface elevation above 2km from the sea level, clear skies and low wind speed, column water vapor less than 0.5cm, the uncertainty in measured atmospheric water vapor profiles less than 30%, the uncertainty in measured atmospheric temperature profiles less than 2 °C, and where surface temperature can be measured at an accuracy better than 0.2 °C for test sites which emissivity is well known. The vicarious calibration experiment with the MAS data and in-situ measurement data collected in the March 1998 Mono Lake field campaign shows that the MAS

calibration accuracy for the split-window channels (at 11 and 12 μ m) has been significantly improved to better than ± 0.3 K in the past three years while the calibration accuracy in other TIR channels needs further improvement. We realize that the spatial variation in surface temperatures of test sites is a major uncertainty source in the in-situ measurements. In order to reduce the uncertainty in measured surface temperatures we will use an IR camera and more TIR thermometers in the future field campaigns. We plan to conduct vicarious calibration activities for MAS and MODIS TIR channels over large flat homogeneous targets at high elevations in the coming years. Ideal candidate sites of such targets include Namco Lake in Tibet (30.75° N, 90.5° E, surface elevation 4718m) and Uyuni Salt Flats in Bolivia (20.25° S, 67.50° W, surface elevation 3810m).

ACKNOWLEDGEMENTS

This work was supported by EOS Program contract NAS5-31370 of the National Aeronautics and Space Administration. We wish to express our gratitude to Greg Cleven and his colleagues at NASA Ames Research Center and the ER-2 Operation Office at NASA Dryden Flight Research Center for the ER-2 flights and MAS data, to Daniel Dawson at Sierra Nevada Aquatic Research Laboratory, and Richard Martin, Death Valley National Park, for research/collecting permit for our field campaign in March 1998, to Mr. Zhi Yiqiao, Institute of Remote Sensing Application, Chinese Academy of Sciences, for his participation in the field campaign under support of the Chinese Climbing Project.

REFERENCES

- Barnes, W. L., T. S. Pagano, and V. V. Salomonson, "Prelaunch characteristics of the Moderate Resolution Imaging Spectroradiometer (MODIS) on EOS-AM1," *IEEE Trans. Geosci. Remote Sens.*, vol. 36, no. 4, pp. 1088-1100, 1998.
- Berk, A., L. S. Bemstein, and D. C. Robertson, "MODTRAN: A moderate resolution model for LOWTRAN," Rep. AFGL-TR-87-0220, Burlington, MA: Spectral Sciences, Inc., 1987.
- Butler, J. J. and R. A. Barnes, "Calibration strategy for the Earth Observing System (EOS)-AM1 platform," *IEEE Trans. Geosci. Remote Sens.*, vol. 36, no. 4, pp. 1056-1061, 1998.
- Esaias, W. E., M. R. Abbott, I. Barton, O. W. Brown, J. W. Campbell, K. L. Carder, D. K. Clark, R. L. Evans, F. E. Hoge, H. R. Gordon, W. P. Balch, R. Letelier, and P. J. Minnett, "An overview of MODIS capabilities for ocean science observations," *IEEE Trans. Geosci. Remote Sens.*, vol. 36, no. 4, pp. 1250-1265, 1998.
- Hale, G. M. and M. R. Querry, "Optical constants of water in the 200-nm to 200- μ m wavelength region," *Appl. Optics*, vol. 12, no. 3, pp. 555-641, 1973.
- Justice, C. O., E. Vermote, J. R. G. Townshend, R. Defries, D. O. Roy, D. K. Hall, V. V. Salomonson, J. L. Privette, G. Riggs, A. Strahler, W. Lucht, R. B. Myneni, K. Knyazikhin, S. W. Running, P. R. Nemani, Z. Wan, A. R. Huete, W. van Leeuwen, R. E. Wolfe, L. Giglio, J.-P. Muller, and Y. Knyazikhin, M. J. Barnsley, "The Moderate

- Resolution Imaging Spectroradiometer (MODIS): land remote sensing for global change research,” *IEEE Trans. Geosci. Remote Sens.*, vol. 36, no. 4, pp. 1228-1249, 1998.
- King, M. D., D. D. Herring, and D. J. Diner, “The Earth Observing System (EOS): A space-based program for assessing mankind’s impact on the global environment,” *Opt. Photo. News*, vol. 6, pp. 34-39, 1995.
- King, M. D., Y. J. Kaufman, W. P. Menzel, and D. Tanré, “Remote sensing of cloud, aerosol, and water vapor properties from the Moderate Resolution Imaging Spectrometer (MODIS),” *IEEE Trans. Geosci. Remote Sens.*, vol. 30, no. 1, pp. 2-27, 1992.
- King, M. D., W. P. Menzel, P. S. Grant, J. S. Myers, G. T. Arnold, S. E. Platnick, L. E. Gumley, S. C. Tsay, C. C. Moeller, M. Fitzgerald, K. S. Brown, and F. G. Osterwisch, “Airborne scanning spectrometer for remote sensing of cloud, aerosol, water vapor and surface properties,” *J. Atmos. Ocean. Technol.*, vol. 13, pp. 777-794, 1996.
- Moeller, C. C., P. S. Grant, D. D. Laporte, L. E. Gumley, P. Hajek, W. P. Menzel, J. S. Myers, and S. White, “Blackbody emissivity considerations for radiometric calibration of the MODIS Airborne Simulator (MAS) thermal channels,” in *NASA’s Earth Observing System, SPIE Conference on 5-6 August, 1996, Denver, CO*, vol. 2820, pp. 44-55, 1996.
- Salomonson, V., W. Barnes, P. Maymon, H. Montgomery, and H. Ostrow, “MODIS: advanced facility instrument for studies of the Earth as a system,” *IEEE Trans. Geosci. Remote Sens.*, vol. 27, no. 2, pp. 145-153, 1989.
- Snyder, W. and Z. Wan, “Surface temperature correction for active infrared reflectance measurements of natural materials,” *Appl. Optics*, vol. 35, no. 13, pp. 2216-2220, 1996.
- Snyder, W., Z. Wan, Y. Zhang, and Y.-Z. Feng, “Requirements for satellite land surface temperature validation using a silt playa,” *Remote Sens. Environ.*, vol. 61, no. 2, pp. 279-289, 1997a.
- Snyder, W., Z. Wan, Y. Zhang, and Y.-Z. Feng, “Thermal infrared (3-14 μm) bidirectional reflectance measurements of sands and soils,” *Remote Sens. Environ.*, vol. 60, pp. 101-109, 1997b.
- Wan, Z. and J. Dozier, “A generalized split-window algorithm for retrieving land-surface temperature from space,” *IEEE Trans. Geosci. Remote Sens.*, vol. 34, no. 4, pp. 892-905, 1996.
- Wan, Z. and Z.-L. Li, “A physics-based algorithm for retrieving land-surface emissivity and temperature from EOS/MODIS data,” *IEEE Trans. Geosci. Remote Sens.*, vol. 35, no. 4, pp. 980-996, 1997.
- Warren, S. G., “Optical constants of ice from the ultraviolet to the microwave,” *Appl. Optics*, vol. 23, no. 8, pp. 1206-1225, 1984.

TABLE I. The central wavelength (λ_c) and bandwidth ($\Delta\lambda$) of MODIS Airborne Simulator (MAS) channels as configured in March 1998 and the equivalent channels of the MODIS onboard the EOS-AM1 platform.

MAS channel	λ_c ($\Delta\lambda$) μm (nm)	MODIS channel	λ_c ($\Delta\lambda$) μm (nm)	MAS channel	λ_c ($\Delta\lambda$) μm (nm)	MODIS channel	λ_c ($\Delta\lambda$) μm (nm)
1	0.470 (39)	3	0.469 (20)	26	3.116 (155)		
2	0.552 (42)	4	0.555 (20)	27	3.274 (149)		
3	0.654 (52)	1	0.645 (50)	28	3.429 (159)		
4	0.704 (43)	14	0.678 (10)	29	3.589 (154)		
5	0.746 (42)	15	0.748 (10)	30	3.745 (140)	20	3.750 (180)
6	0.828 (44)			31	3.905 (152)	22	3.959 (60)
7	0.870 (42)	2	0.858 (35)	32	4.064 (151)	23	4.059 (60)
8	0.912 (41)	17	0.905 (30)	33	4.222 (157)		
9	0.952 (41)	19	0.940 (50)	34	4.372 (165)	24	4.465 (65)
10	1.620 (52)	6	1.640 (24)	35	4.536 (149)	25	4.515 (67)
11	1.674 (52)			36	4.690 (158)		
12	1.728 (52)			37	4.848 (149)		
13	1.780 (52)			38	4.997 (142)		
14	1.832 (50)			39	5.149 (145)		
15	1.884 (52)			40	5.295 (142)		
16	1.932 (52)			41	5.410 (93)		
17	1.984 (54)			42	8.467 (302)	29	8.550 (300)
18	2.036 (57)			43	9.672 (529)	30	9.730 (300)
19	2.084 (55)			44	10.467 (440)		
20	2.134 (56)	7	2.130 (50)	45	10.975 (490)	31	11.030 (500)
21	2.182 (55)			46	11.969 (420)	32	12.020 (500)
22	2.232 (57)			47	12.860 (410)		
23	2.282 (55)			48	13.274 (460)	33	13.335 (300)
24	2.332 (56)			49	13.813 (560)	35	13.935 (300)
25	2.380 (56)			50	14.266 (430)	36	14.235 (300)

TABLE II. Mean and standard deviation of band brightness temperature (T_b) in seven MAS bands over four flat homogeneous study areas in the Mono Lake field campaign on March 10, 1998.

MAS band no.	band center (μm)	T_b (δT_b)	T_b (δT_b)	T_b (δT_b)	T_b (δT_b)	estimated		
		($^{\circ}\text{C}$) ice-covered GL 16x16	($^{\circ}\text{C}$) snow-covered GL 16x16	($^{\circ}\text{C}$) Mono Lake 80x80	($^{\circ}\text{C}$) snow site 16x16	$NE\Delta T_{\min}$	$NE\Delta T_{\max}$	($^{\circ}\text{C}$)
30	3.745	-1.49 (1.46)	1.53 (1.29)	2.78 (1.27)	2.57 (1.41)	0.9-1.2		
31	3.905	-2.86 (1.14)	-1.40 (1.08)	1.79 (0.96)	-0.69 (1.16)	0.6-0.9		
32	4.064	-5.13 (1.39)	-4.28 (1.45)	-0.44 (1.27)	-4.14 (1.54)	0.9-1.2		
42	8.467	-3.00 (0.22)	-2.90 (0.22)	1.87 (0.34)	-2.87 (0.25)			0.1
45	10.975	-1.56 (0.25)	-1.42 (0.25)	3.97 (0.38)	-1.37 (0.30)			0.2
46	11.969	-2.81 (0.42)	-2.04 (0.51)	3.78 (0.49)	-2.28 (0.53)			0.3
48	13.274	-10.53 (0.68)	-9.82 (0.63)	-6.23 (0.71)	-10.05 (0.74)			0.5

TABLE III. The effects of uncertainties in atmospheric profiles on the TOA T_b values for a ice-covered lake surface at $T_s = -0.5^{\circ}\text{C}$ according to MODTRAN3.5 simulations.

MAS band no.	band center (μm)	calculated T_b (sensitivity to $\delta(cwv)$ and δT_a)		
		measured profiles cwv=0.32cm	cwv=0.64cm no change in T_a	$T_a + 2^{\circ}\text{C}$ no change in cwv
30	3.745	-1.30	-1.33 (-0.03)	-1.21 (0.09)
31	3.905	-2.03	-2.03 (0.00)	-1.91 (0.12)
32	4.064	-3.45	-3.45 (0.00)	-3.17 (0.28)
42	8.467	-2.36	-2.49 (-0.13)	-2.16 (0.20)
45	10.975	-1.65	-1.64 (0.01)	-1.60 (0.05)
46	11.969	-3.44	-3.36 (0.08)	-3.38 (0.06)
48	13.274	-12.55	-12.49 (0.06)	-11.98 (0.57)

TABLE IV. The effect of the emissivity values on the MAS calibration in the ice-covered lake case.

MAS band no.	band center (μm)	ε used in 1B calibration	1B T_b ($^{\circ}\text{C}$)	measured ε of the black paint	recalibrated T_b ($^{\circ}\text{C}$)	δT_b ($^{\circ}\text{C}$)
30	3.745	0.98	-1.49	0.964	-1.25	0.24
31	3.905	0.98	-2.86	0.964	-2.59	0.27
32	4.064	0.98	-5.13	0.964	-4.80	0.33
42	8.467	0.94	-3.00	0.956	-3.24	-0.24
45	10.975	0.94	-1.56	0.951	-1.70	-0.14
46	11.969	0.94	-2.81	0.953	-2.99	-0.18
48	13.274	0.94	-10.53	0.958	-10.95	-0.42

TABLE V. The calibration error (δT_b) in seven MAS TIR bands estimated by comparison with the results of MODTRAN3.5 simulations for the four flat homogeneous study areas under the measured atmospheric profile at zenith viewing angle θ_v .

MAS band no.	band center (μm)	in-situ measurement derived T_b ($^{\circ}\text{C}$)	original T_b (δT_b) ($^{\circ}\text{C}$)	recalibrated T_b (δT_b) ($^{\circ}\text{C}$)
snow-cover site at measured $T_s = -0.84^{\circ}\text{C}$ ($\theta_v = 17^{\circ}$ and solar angle = 42.3°)				
30	3.745	-1.32 to 4.55	2.57	2.71
31	3.905	-2.00 to 1.35	-0.69	-0.47
32	4.064	-3.20 to -1.36	-4.14	-3.83
42	8.467	-2.12	-2.87 (-0.75)	-3.11 (-0.99)
45	10.975	-1.62	-1.37 (0.27)	-1.51 (0.11)
46	11.969	-2.47	-2.28 (0.19)	-2.46 (0.01)
48	13.274	-10.39	-10.05 (0.34)	-10.45 (-0.06)
snow-covered Grant Lake surface at $T_s = -0.84^{\circ}\text{C}$ ($\theta_v = 23^{\circ}$)				
30	3.745	-1.08	1.53	1.69
31	3.905	-1.90	-1.40	-1.16
32	4.064	-3.20	-4.28	-3.97
42	8.467	-2.16	-2.90 (-0.74)	-3.13 (-0.97)
45	10.975	-1.63	-1.42 (0.21)	-1.56 (0.07)
46	11.969	-2.47	-2.02 (0.45)	-2.21 (0.26)
48	13.274	-10.58	-9.82 (0.76)	-10.22 (0.36)
ice-covered Grant Lake surface at $T_s = -0.7^{\circ}\text{C}$ ($\theta_v = 23^{\circ}$)				
30	3.745	-1.16	-1.49 (-0.33 ?)	-1.25 (0.09 ?)
31	3.905	-1.96	-2.86 (-0.90 ?)	-2.59 (-0.63 ?)
32	4.064	-3.27	-5.13 (-1.86 ?)	-4.80 (-1.53 ?)
42	8.467	-2.34	-3.00 (-0.66)	-3.24 (-0.90)
45	10.975	-1.79	-1.56 (0.23)	-1.70 (0.09)
46	11.969	-3.57	-2.81 (0.76)	-2.99 (0.58)
48	13.274	-12.10	-10.53 (1.57)	-10.95 (1.15)
Mono Lake surface at $T_s = 4.6^{\circ}\text{C}$ ($\theta_v = 1.4^{\circ}$)				
30	3.745	3.96	2.78 (-1.16)	2.91 (-1.05)
31	3.905	3.11	1.79 (-1.32)	1.95 (-1.16)
32	4.064	1.47	-0.44 (-1.91)	-0.24 (-1.71)
42	8.467	2.55	1.87 (-0.68)	1.73 (-0.82)
45	10.975	3.84	3.97 (0.13)	3.90 (0.06)
46	11.969	3.61	3.78 (0.17)	3.70 (0.09)
48	13.274	-7.23	-6.23 (1.00)	-6.54 (0.69)

TABLE VI. Comparison of the calibration error (δT_b) in the closely corresponding TIR bands of the MAS configurations in March 1998 and 1995.

MAS band no.	band center (μm)	δT_b (K) March 1998 (this study)	δT_b (K) August 1995 (King et al, 1996)	δT_b (K) May 1995 (Moeller et al, 1996)
30	3.745	-1.1		
31	3.905	-1.2	-1.4 (3.90 μm)	
32	4.064	-1.7		
42	8.467	-0.8	-0.9 (8.60 μm)	-0.47 (8.59 μm)
45	10.975	within ± 0.3 (± 0.15)	-0.6 (11.02 μm)	-0.50 (11.01 μm)
46	11.969	within ± 0.3 (± 0.15)	-0.5 (11.96 μm)	-0.13 (11.97 μm)
48	13.274	0.7		

TABLE VII. Error analysis of the snow surface temperatures determined by the MIDAC TIR spectrometer in MAS channels 42 and 45.

uncertainty source source	δT ($^{\circ}\text{C}$)	comments
calibration error of the spectrometer	≤ 0.15	traceable to NIST standard by thermistors
$\delta\epsilon$ of the snow surface	≤ 0.15	$\delta\epsilon \leq 0.0025$
δT_s of the snow surface	≈ 0.2	referred from MAS data (see Table II)
rms	≤ 0.3	

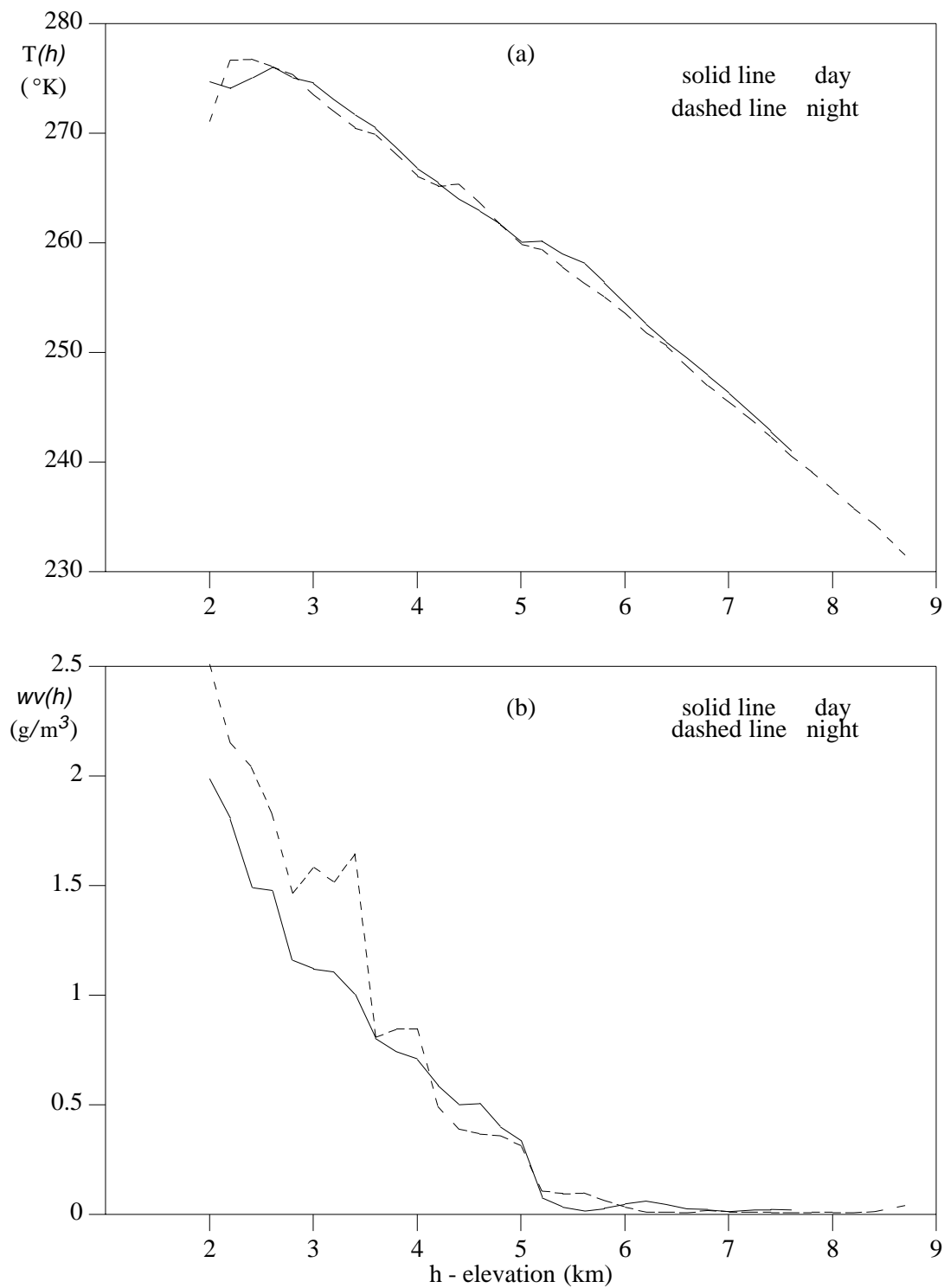


Fig. 1, Atmospheric temperature (a) and water vapor (b) profiles near Mono Lake, March 10, 1998.

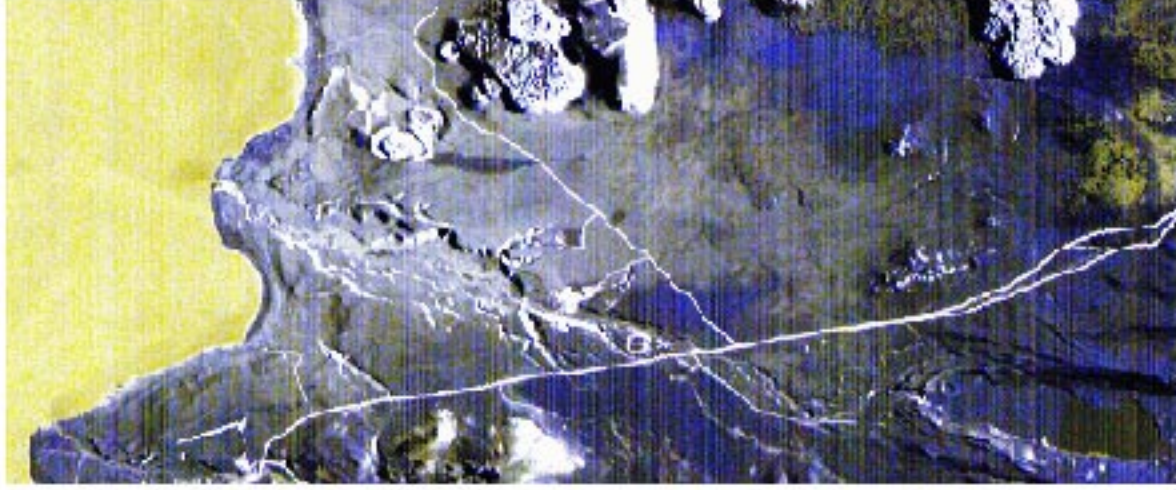
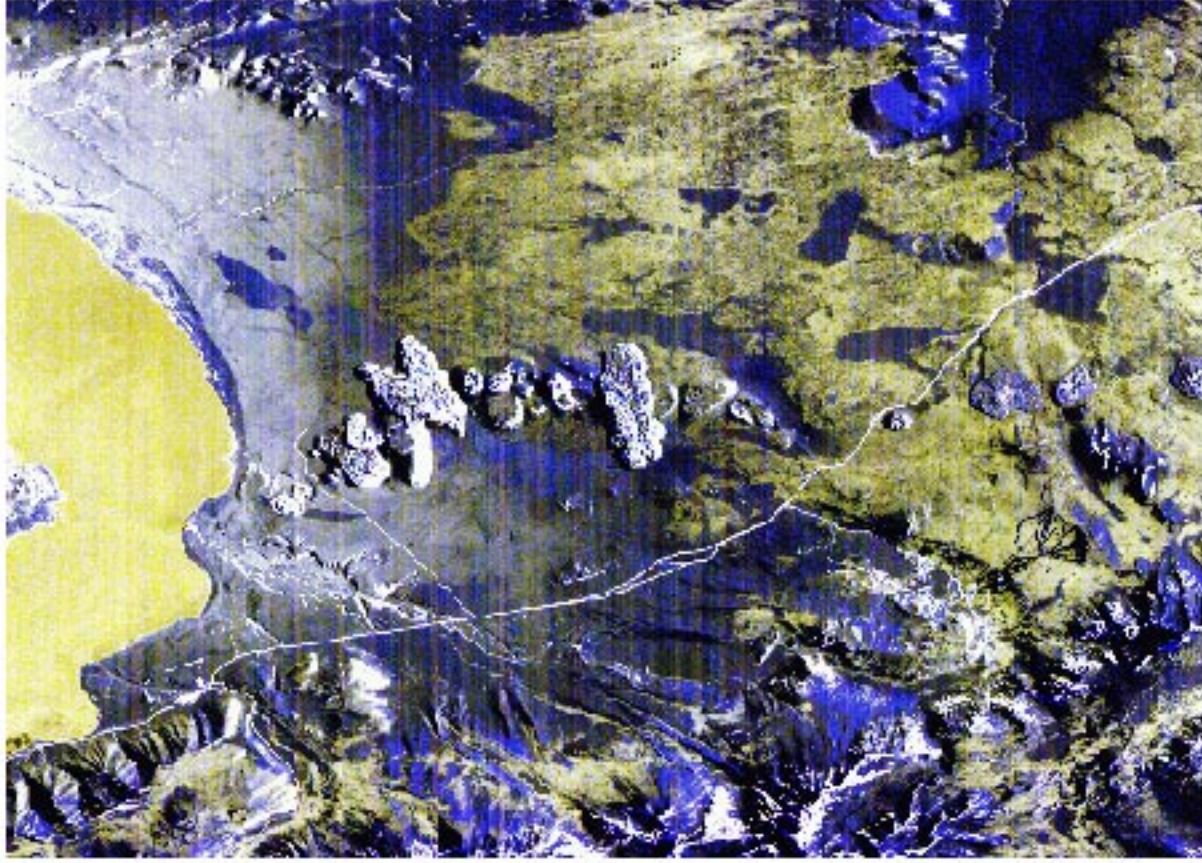


Fig. 2, (a) color composite with enhanced MAS bands 45, 42 and 30 as R, G and B in Moon Lake area (1000 lines by 716 pixels), (b) its sub-area to show four test sites.

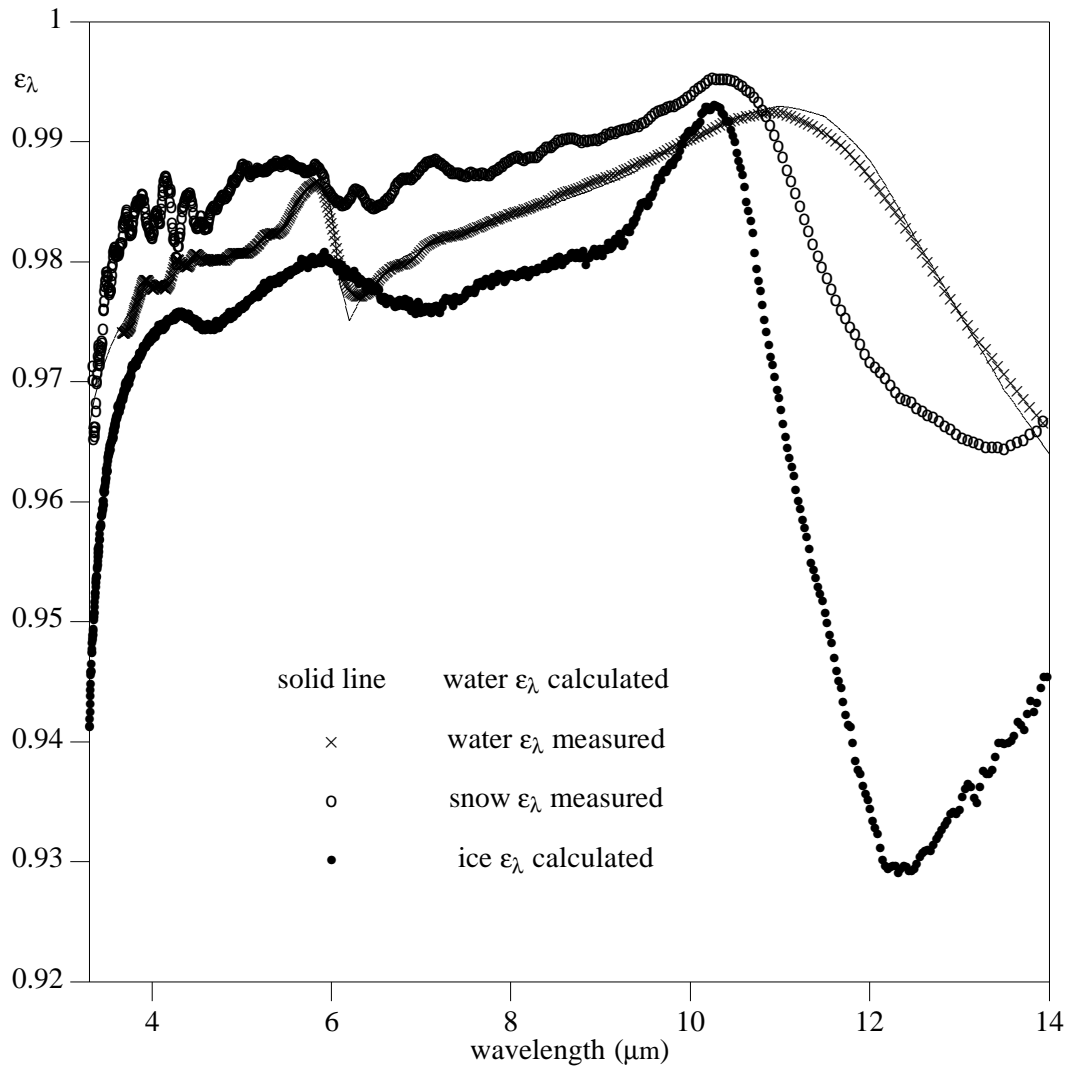


Fig. 3, Spectral emissivities of water, snow, and ice in the 3.3-14 μm region.